Radio Frequency and Linearity Performance of Transistors Using High-Purity Semiconducting Carbon Nanotubes

Chuan Wang,[†,⊥] Alexander Badmaev,[†,⊥] Alborz Jooyaie,[§,⊥] Mingqiang Bao,[‡] Kang L. Wang,[‡] Kosmas Galatsis,[§,*] and Chongwu Zhou[†,*]

[†]Department of Electrical Engineering, University of Southern California, Los Angeles, California 90089, United States, [‡]Department of Electrical Engineering, University of California, Los Angeles, California 90095, United States, and [§]Aneeve Nanotechnologies LLC, UCLA California Nanosystems Institute, Los Angeles, California 90095, United States. [⊥]These authors contributed equally to this work.

ABSTRACT This paper reports the radio frequency (RF) and linearity performance of transistors using high-purity semiconducting carbon nanotubes. High-density, uniform semiconducting nanotube networks are deposited at wafer scale using our APTES-assisted nanotube deposition technique, and RF transistors with channel lengths down to 500 nm are fabricated. We report on transistors exhibiting a cutoff frequency (f_t) of 5 GHz and with maximum oscillation frequency (f_{max}) of 1.5 GHz. Besides the cutoff frequency, the other important figure of merit for the RF transistors is the device linearity. For the first time, we report carbon nanotube RF transistor linearity metrics up to 1 GHz. Without the use of active probes to provide the high impedance termination, the measurement bandwidth is therefore not limited, and the linearity measurements can be conducted at the frequencies where the transistors are intended to be operating. We conclude that semiconducting nanotube-based transistors are potentially promising building blocks for highly linear RF electronics and circuit applications.

KEYWORDS: carbon nanotubes · nanotube separation · semiconducting · radio frequency transistors · linearity

The application of single-walled carbon nanotubes in advanced electronics has been heavily exploited for over a decade. This interest stems from the fact that carbon nanotubes offer a combination of small size, high mobility, ballistic transport, large current density, and low intrinsic capacitance.[1−5] They have been used extensively to demonstrate various kinds of integrated circuits such as logic gates, ring oscillators, and decoders.[6−11] However, due to the coexistence of both metallic and semiconducting nanotubes, the on/off ratio is typically very small for the as-made transistors using a large number of nanotubes,[12−14] and various techniques including electrical breakdown,[15] stripe patterning,[11] or using presorted semiconducting nanotubes[16−18] are necessary in order to boost the on/off ratio of transistors significantly. Therefore, for the carbon nanotubes, instead of digital circuit applications, a more realistic application is the high-performance analog or radio frequency (RF) devices, where manufacturing tolerances are relaxed and the performance metrics required are more suited to the materials and device properties of nanotubes, especially since the transistors do not need to be fully turned off.

Previously, many groups have investigated the potential of using carbon nanotubes for RF applications and have demonstrated the operation of those transistors in the gigahertz frequency range.[19−23] However, in those reports, mainly chemical vapor deposition (CVD)-grown nanotubes, which consist of mixed metallic and semiconducting nanotubes, are used. The existence of the metallic nanotubes causes leakage current in the off-state and results in low on/off ratios. Although for analog/RF application, the on/off ratio is not as crucial as for digital applications, low on/off ratio can still result in low efficiency for applications such as power amplifiers and degrade the transconductance (g_m) and cutoff frequency (f_t) of the RF transistors.

Recent reports have shown that the semiconducting nanotubes can be separated from the metallic nanotubes using density gradient ultracentrifugation, resulting in nanotube solution with up to 99% semiconducting nanotube purity.[24,25] By using such prepurified semiconducting nanotubes, the RF performance is expected to be further improved. With semicondcuting nanotubes assembled by dielectrophoresis,[26] RF transistors with an impressive cutoff frequency of 80 GHz have been demontrated by Happy

* Address correspondence to chongwuz@usc.edu, kos@ee.ucla.edu.

Received for review March 10, 2011 and accepted April 19, 2011.

Published online April 25, 2011
10.1021/nn200919v

and co-workers.[21] Despite the significant progress, there is still room for further improvement in terms of scalability. We have previously reported an aminopropyltriethoxysilane (APTES)-assisted separated nanotube deposition technique that is capable of depositing high-density and uniform semiconducting nanotube thin films at complete wafer scale.[17,18] In this regard, it would be interesting to investigate the performance of nanotube RF transistors fabricated using such scalable platforms. In this work, we have demonstrated that such RF transistors can be fabricated at complete wafer scale, and electrical characterization reveals that such devices also exhibit large transconductance, current drive, and gigahertz operation.

Moreover, it is also important to point out that other than f_t, another even more important figure of merit for RF transistors is the device linearity. It is crucial to not only amplifying signals at high frequency but also amplifying signals linearly in order to maintain the fidelity of the signals. Linearity is also an extremely important property in signal-rich environments due to interference and intermodulation from other communication bands and channels. Transistors based on one-dimensional (1D) materials have recently been predicted to offer much better linearity characteristics than traditional bulk devices, which is fundamentally due to the combination of the unique 1D transport properties and the 1D density of states of carriers in the transistor channel.[27] To test the linearity of the nanotube transistor, there have been few studies where a common source configuration nanotube transistor loaded with a high impedance resistor on the drain, terminated with a high impedance active probe, has been driven with two low-frequency tones to characterize the circuit's harmonic distortion.[28] However, since the active probes are used in the study to provide the high impedance termination required for the low current drive nanotube devices, the operational bandwidth is small, limited to order of kilohertz, and the measured nonlinearity metrics are not valid for the frequencies under which the nanotube transistors are intended to be implemented and operated at (*i.e.*, gigahertz frequency).

In this paper, we have, to the best of our knowledge, for the first time, characterized the key device linearity metrics with standard 50 Ω terminations and conducted the two-tone test of the nanotube RF devices at gigahertz frequency, which is the intended operating frequency of the transistor. We performed nonlinearity measurements using both single-tone and two-tone, where major device linearity figures of merits such as the −1 dB gain compression point (P1dB) and input/output third-order intercept points (IIP3/OIP3 or ITOI/OTOI) were extracted. Our work shows that, in line with theoretical predictions, the semiconducting nanotube-based transistors are promising building blocks for future highly linear RF electronics and circuits.

RESULTS AND DISCUSSION

Figure 1a illustrates the fabrication process and shows the schematic of the completed separated nanotube RF transistor. Details about the device fabrication process can be found in the Methods section. The RF transistors are fabricated on a highly resistive silicon wafer ($\rho > 5$ kΩ·cm) with 200 nm SiO_2 to ensure minimum parasitics from the substrates. Aluminum back-gates with a thermally oxidized Al_2O_3 gate dielectric are used as the gate stacking instead of the traditional top-gate structure with a high-κ dielectric such as Al_2O_3 and HfO_2 deposited by atomic layer deposition (ALD). The advantage is that the thermal oxidization of Al to form Al_2O_3 is a self-limiting process, resulting in a high-quality, ultrathin gate dielectric, which leads to better gate strength and larger transconductance. In contrast, it is very difficult to obtain a leakage-free Al_2O_3 dielectric with such small thickness using ALD. As a next step, high density and uniform separated 95% semiconducting nanotubes (IsoNanotubes-S from NanoIntegris, Inc.) with an average length of 1 μm are deposited using the APTES-assisted separated nanotube deposition technique as discussed in our previous publications.[17,18] For the source/drain metal contacts, palladium is used due to its large work function, which offers Schottky-barrier-free contacts to the nanotubes for hole injection.[5]

The above-described APTES-assisted separated nanotube deposition method and the RF transistor fabrication process is scalable and can thus be performed at wafer scale. A 3 in. wafer with the RF transistors is shown in Figure 1b. The optical microscope image of the separated nanotube RF transistor is shown in Figure 1c, where the device is configured into the ground−signal−ground (GSG) coplanar waveguide structure so that we can perform microwave measurements. The device contains a pair of nanotube channels with a channel width of 500 μm and a channel length of 500 nm. Figure 1d is a zoom-in optical microscope image, where we can clearly identify two pairs of channels, the Ti/Au pads, Al back-gate and Ti/Pd source/drain extensions. The SEM image of the device channel region after nanotube deposition is shown in Figure 1e. The strip in the center corresponds to the aluminum back-gate, and the top and bottom metal electrodes are the Ti/Pd source/drain extensions. The channel length is 500 nm, and one can find that the channel is covered by a high-density semiconducting nanotube network.

We have first characterized the DC performance of the separated nanotube RF transistors, and the results are summarized in Figure 2. Figure 2a is the transfer characteristics ($I_{DS}-V_{GS}$ curves) measured at various

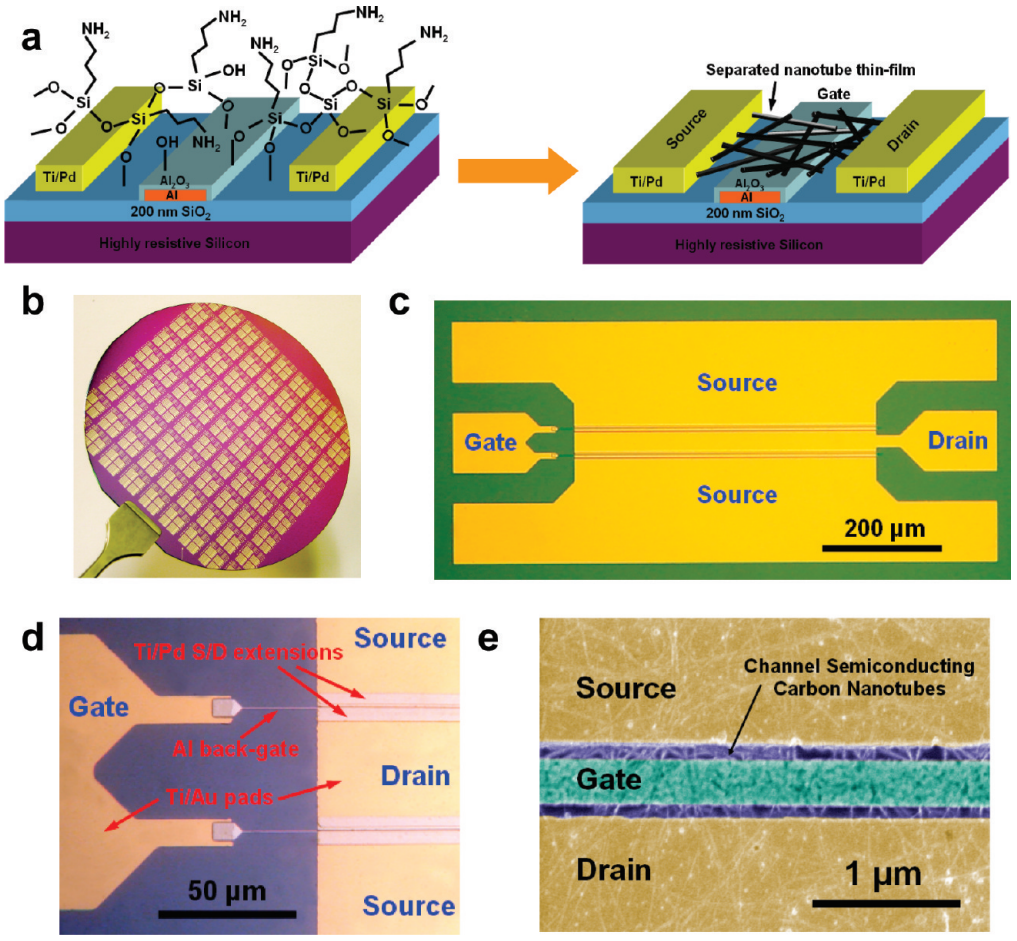

Figure 1. Scalable fabrication of the aluminum back-gated separated nanotube RF transistors. (a) Schematic showing the APTES-assisted separated nanotube deposition process for the separated nanotube RF transistor fabrication. (b) Wafer of the separated nanotube RF transistors. (c) Optical microscope image of the nanotube RF transistor. (d) Zoom-in optical microscope image showing two pairs of channels, the aluminum back-gate, and Pd S/D extensions of the nanotube RF transistor. (e) SEM image showing the channel of the device with a channel length of 500 nm.

drain voltages (V_{DS}) for one channel of the nanotube RF transistor with $W = 500$ μm and $L = 500$ nm. From the curves, one can find that the on-state current of the device (I_{on}) measured at $V_{DS} = -1$ V and $V_{GS} = -2$ V is 9.06 mA, which corresponds to an on-state current density (I_{on}/W) of 18.12 μA/μm. The off-state current (I_{off}) measured at $V_{DS} = -1$ V and $V_{GS} = 2$ V is 1.93 mA, so that we can calculate the on/off ratio of the device to be 4.69. The device cannot be completely depleted due to the 500 nm channel length used. As reported in our previous publication, for devices using 95% semiconducting nanotubes, the on/off ratio is heavily dependent on the device channel length.[17,18] As the channel length decreases, the on/off ratio decreases, and the on/off ratio is always below 10 when a channel length of less than 4 μm is used. Using either longer channel length (>10 μm) or separated nanotube solution with even higher purity (*e.g.*, 99%) of semiconducting nanotubes would lead to a significant improvement in on/off ratio but also with a significantly reduced transconductance.[18] In principle, by using semiconducting nanotubes with higher purity, the device transconductance and thus RF performance should be improved, considering that the nanotubes are still exactly the same as the lower purity sample in terms of length, diameter, and band gap. However, for the nanotube samples we used in this study, higher-purity semiconducting nanotubes (98 and 99%) tend to have shorter length compared with lower purity ones (95%). Therefore, although the transistors using 98% semiconducting nanotubes exhibit much better on/off ratio, the on-current density and transconductance are, in fact, lower than the transistors using 95% semiconducting nanotubes by a factor of 3–7.[18] This trade-off between on/off ratio and transconductance can be attributed to more tube-to-tube junctions resulting from shorter nanotubes. On the basis of the discussion above, our choice of using 95% semiconducting nanotubes is justified because transconductance is the most crucial parameters for the RF device instead of the on/off ratio.

Figure 2b shows the g_m–V_{GS} curve derived from the I_{DS}–V_{GS} characteristics. The maximum g_m is measured to be 2.81 mS when V_{GS} is around 0 V, and the

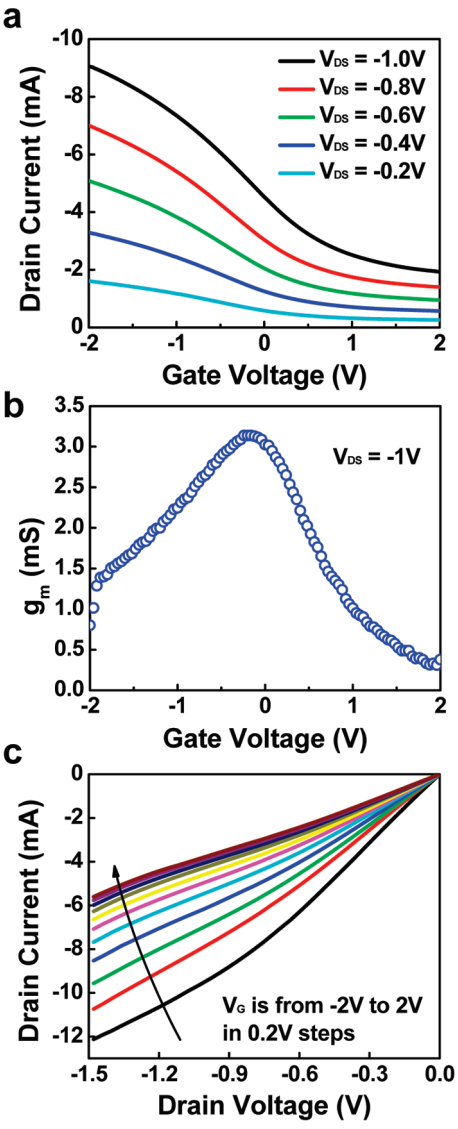

Figure 2. DC characteristics of the separated nanotube RF transistors. (a) Transfer characteristics ($I_{DS}-V_{GS}$) of the separated nanotube RF transistor (L = 0.5 μm, W = 500 μm) measured at various V_{DS}. (b) g_m-V_{GS} characteristics measured at $V_{DS} = -1$ V. (c) Output ($I_{DS}-V_{DS}$) characteristics measured at various V_{GS} from -2 to 2 V.

corresponding g_m/W is 6.28 μS/μm. Figure 2c is the output characteristics ($I_{DS}-V_{DS}$ curves) of the device measured under different gate biases. We can see that the $I_{DS}-V_{DS}$ curves appear to be linear at low drain biases, indicating that ohmic contacts instead of Schottky contacts are formed between the metal electrodes and the nanotubes. Under higher biases, the current begins to saturate, and the saturation behavior is superimposed on the metallic behavior of the nanotube RF transistor. This leads to improved R_{out}, which is useful in order to obtain a voltage gain.

We have further characterized the RF performance of the separated nanotube transistor using vector network analyzer (VNA), and the measurement setup is shown in Figure 3a. The sources are grounded, and the DC biases are supplied to the gate and drain terminal through the bias-T. For the RF measurement, the gate is biased at $V_{GS} = 0$ V and the drain is biased at $V_{DS} = -1$ V, as this is the bias condition that gives the maximum g_m, as confirmed by the DC measurement. The measured S parameters from 50 MHz to 5 GHz are plotted in Figure 3b. From the S parameters, we can further derive the h_{21}, which corresponds to the current gain, and the maximum available gain (G_{max}) using the following equations[22]

$$h_{21} = \frac{-2S_{21}}{(1 - S_{11})(1 + S_{22}) + S_{12}S_{21}} \quad (1)$$

$$G_{max} = \left|\frac{S_{21}}{S_{12}}\right| \text{ for } K < 1 \text{ or}$$

$$G_{max} = \left|\frac{S_{21}}{S_{12}}(K - \sqrt{K^2 - 1})\right| \text{ for } K > 1 \quad (2)$$

where K is the stability factor that can be calculated using the following equation

$$K = \frac{1 + |S_{11}S_{22} - S_{12}S_{21}|^2 - |S_{11}|^2 - |S_{22}|^2}{2|S_{12}S_{21}|} \quad (3)$$

The derived h_{21} (red trace) and G_{max} (green trace) are plotted as a function of frequency in Figure 3c. From the figure, one can find that, at 1 GHz, the current gain h_{21} drops to 0 dB. So the as-measured (*i.e.*, extrinsic) cutoff frequency ($f_{t\_extrinsic}$) of the separated nanotube RF transistor is 1 GHz. From the G_{max} curve, we can also find that the unity power gain frequency f_{max} is 1.5 GHz.

The extrinsic cutoff frequency of the transistor is largely affected by the parasitic capacitance, and if we perform short-open-load-through (SOLT) de-embedding, we can rule out the effect from the parasitic capacitance and deduce the intrinsic cutoff frequency ($f_{t\_intrinsic}$) of the separated nanotube RF transistor. In particular, considering the small size of the nanotubes in the channel in comparison with the GSG pads incorporated for probing measurement, the parasitic capacitance could strongly degrade the corresponding AC performance. On the basis of the SOLT de-embedding scheme discussed in the Supporting Information (Figure S1), we have deduced the intrinsic h_{21} of the separated nanotube RF transistor plotted as the blue trace in Figure 3c. From the figure, the intrinsic cutoff frequency is derived to be 5 GHz. The frequency response of the separated nanotube RF transistor is significantly better than the transistor using CVD-grown aligned carbon nanotubes with exactly the same device geometry as shown in the Supporting Information (Figure S2). The improvement can be attributed to the improved g_m as a result of the high-purity semiconducting nanotubes used.

The gate bias dependence of the cutoff frequency is illustrated in Figure 3d, and more information can be

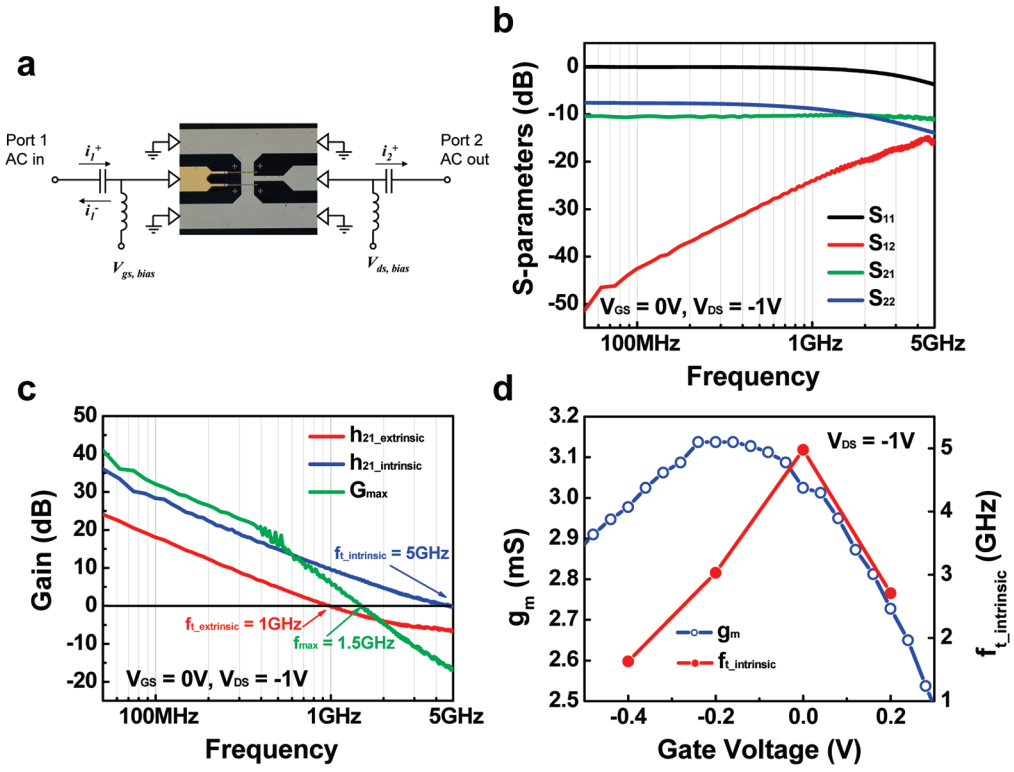

Figure 3. RF characteristics of the separated nanotube RF transistors. (a) Schematic showing the RF measurement setup. (b) As-measured *S* parameters for the separated nanotube RF transistor (dual channel with $L = 0.5\ \mu m$, $W = 500\ \mu m$) from 50 MHz to 5 GHz. The transistor is biased at $V_{GS} = 0$ V and $V_{DS} = -1$ V for maximum g_m. (c) Extrinsic and intrinsic current gain h_{21}, and maximum available gain G_{max} derived from the measured *S* parameters from 50 MHz to 5 GHz. (d) Transconductance and intrinsic cutoff frequency as a function of V_{GS}.

found in the Supporting Information (Figure S3). As the gate voltage varies from −0.4 to 0.2 V, the measured cutoff frequency of the device also varies and peaks at $V_{GS} = 0$ V. The variation of f_t follows the variation of g_m since f_t is proportional to g_m. The shift of around 0.24 V between the g_m and f_t curves can be attributed to the device hysteresis as shown in the Supporting Information (Figure S4). Furthermore, owing to the uniformity of the separated nanotube thin film deposited using APTES, the transistors also behave uniformly. For the six transistors for which we characterized the RF performance, the deduced intrinsic f_t values under the optimal bias conditions only vary from 3.05 to 4.98 GHz, and the average performance from those transistors is 3.86 GHz.

Besides the cutoff frequency, linearity is another important figure of merit for RF transistors. We have performed both single-tone and two-tone measurements using the test bench setup illustrated in Figure 4a. Since our separated nanotube RF transistors provide high current drive, on the order of 10−20 mA, we do not need to resort to high-impedance probes or terminations as opposed to the previous report.[28] Consequently, the measurement bandwidth is not limited. For the measurement, two tones at adjacent frequencies are applied to the gate of the nanotube RF transistors through a power combiner. The two tones are applied all the way up to the extrinsic f_t limit of the nanotube RF transistors, as reported below, and not just in the kilohertz and sub-kilohertz range in the previous report.[28] Besides, despite the high current drive and g_m of our separated nanotube RF transistors, we decided not to focus on the gain from the device, as we chose to incorporate standard 50 Ω terminations (for both the spectrum analyzer and the load) in order to observe the high-frequency behavior of the device. Nevertheless, it is worth noting that the absence of gain may affect the linearity measurement in the circuit level since the output signal level is limited. Possible solutions to this issue include increasing the nanotube density in order to improve g_m/W or further enlarging the device channel width. In order to achieve gain from the transistors directly driving 50 Ω loads, $g_m \times R_{out}$ should be greater than 1, where the total impedance seen at the output node (R_{out}) equals the output resistance of the transistor (r_o) in parallel with the input impedance of the measurement instrument (50 Ω) and the 50 Ω load resistor. Assuming r_o is much larger than 50 Ω, R_{out} is therefore approximately 25 Ω, which means that the device transconductance needs to be larger than 40 mS so that $g_m \times 25 > 1$. We are currently working on the above proposed solutions to further increase the transconductance in order to obtain gain from the transistors.

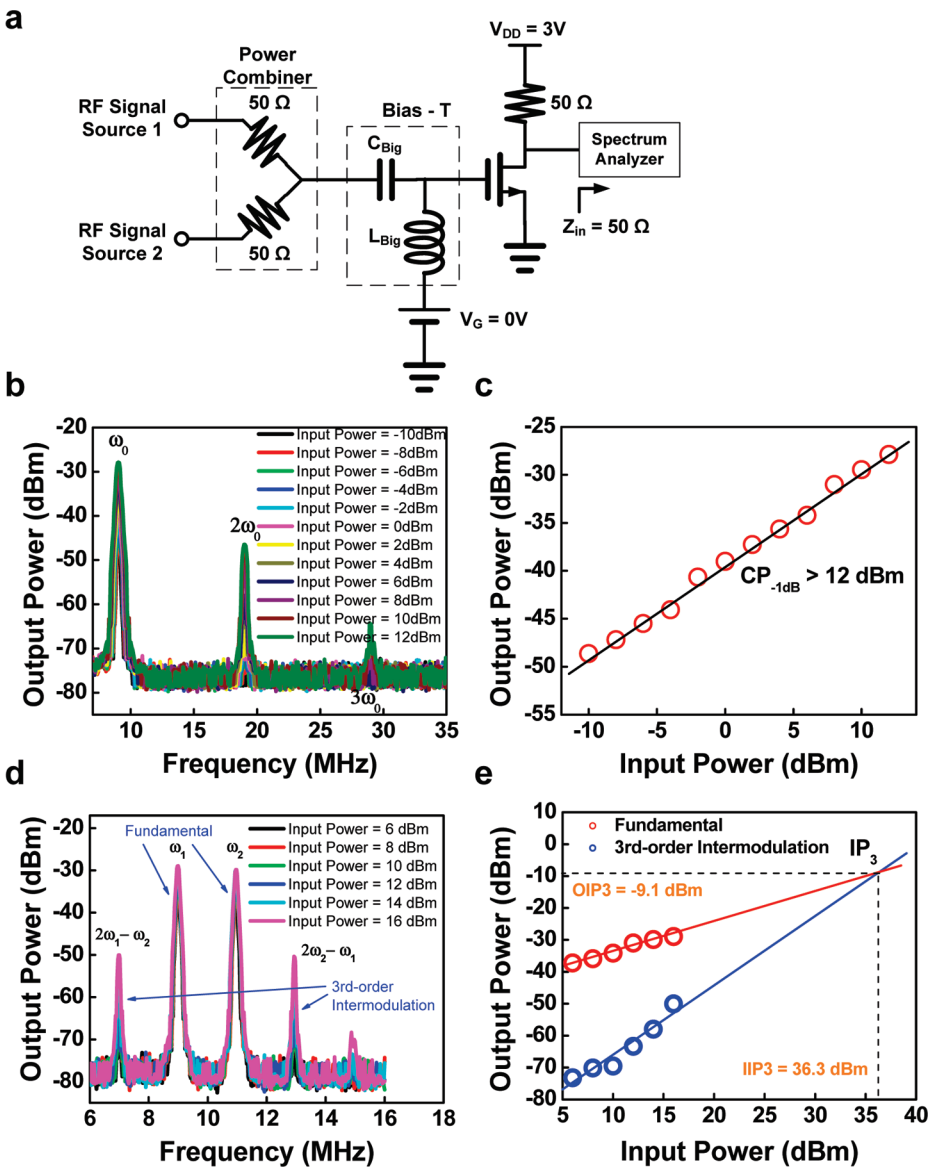

Figure 4. Linearity characteristics of the separated nanotube RF transistors. (a) Schematic showing the two-tone measurement setup to capture the nonlinearity of the separated nanotube RF transistors. (b) Single-tone harmonic distortion characterization results showing the output spectrum of the device with various input power levels from −10 to 12 dBm. (c) Output power of the fundamental as a function of input power to extract the 1 dB gain compression point (P1dB). (d) Two-tone intermodulation characterization results showing the output spectrum with various input power levels from 6 to 16 dBm. (e) Output power of the fundamental and third-order intermodulation as a function of the input power to extract the IIP3 and OIP3.

For the linearity measurement, the device is characterized for single-tone (second-order and third-order harmonic distortion for 1 dB compression point) as well as two-tone intermodulation distortion (third-order intercept point analysis). Figure 4b shows the results of the single-tone measurement, where the separated nanotube RF transistor biased with $V_{GS} = 0$ V (for peak g_m and f_T) and $V_{DS} = -1$ V is driven with a single tone of varying power levels at 9 MHz. From the output spectrum captured using the spectrum analyzer, one can find the fundamental (ω_0), the second-order ($2\omega_0$), and third-order ($3\omega_0$) harmonic components. If we extract the output power of the fundamental from Figure 4b and plot it as a function of input power, we can obtain the compression point plot as shown in Figure 4c. This figure indicates that the output power increases linearly as the input power up to 12 dBm, and no gain compression can be observed. This means that the P1dB of the separated nanotube RF transistor is above 12 dBm; that is, the device operates linearly up to an input power of 12 dBm (~16 mW).

Figure 4d illustrates the intermodulation distortion performance of our separated nanotube RF transistors in accordance with the test-bench presented in Figure 4a. We conducted the two-tone test with two tones at 9 MHz (ω_1) and 11 MHz (ω_2) to ensure the

third-order intermodulations ($\omega_1 + 2\omega_2$ and $2\omega_1 + \omega_2$) that fall close to the tones are observable and measurable accurately. On the basis of Figure 4d, the power level of the fundamentals and third-order intermodulations are extracted and are plotted as a functional of input power (Figure 4e). In theory, as the input power increases, the power of the third-order intermodulations increases 3 times faster than the fundamental. Therefore, we can perform extrapolation and find the point where the power of the third-order intermodulation is equal to the power of the fundamental. This is the so-called third-order intercept point, and the corresponding input and output power levels are defined as IIP3 and OIP3. From Figure 4e, the IIP3 is measured to be 36.3 dBm (~4.3 W) and the OIP3 is measured to be −3.3 dB (~0.5 mW) for the separated nanotube RF transistors. We have also performed the intermodulation distortion measurements at frequencies near the f_t limit (1 GHz) of the separated nanotube RF transistors, and the results are shown in the Supporting Information (Figure S5). The result indicates that the power gain does not decrease much even when the input frequency is at 1 GHz, and the third-order intermodulations are much lower (below the noise floor) at this frequency.

As a conclusion, we have demonstrated the scalable fabrication of RF transistors with cutoff frequency up to 5 GHz using separated nanotube networks. With direct 50 Ω termination, the linearity figures of merit of the transistors including P1dB and IP3 have been characterized, for the first time, at the frequencies where the transistors are intended to be operating. Our work reveals that the semiconducting nanotube-based transistors are potentially promising building blocks for future highly linear RF electronics and circuits.

METHODS

Separated Nanotube RF Transistor Fabrication. The substrate is chosen to be a highly resistive silicon wafer ($\rho > 5$ kΩ·cm) with 200 nm SiO_2 to ensure minimum parasitics from the substrates. Titanium/gold (0.5/50 nm) probing pads are first patterned using contact aligner and lift-off process. After that, aluminum back-gates (40 nm) are patterned using e-beam writing, and the sample is heated to 200 °C in oxygen to oxidize the surface of the aluminum to form 2−3 nm Al_2O_3 as gate dielectric. The sample is then immersed into diluted APTES solution (1% APTES in isopropyl alcohol (IPA)) for 10 min to functionalize the substrate with amine-terminated monolayer. After that, the sample is rinsed with IPA, blown dry thoroughly, and then immersed into the commercially available 0.01 mg/mL separated nanotube solution with 95% semiconducting nanotubes (NanoIntegris Inc.) for 30 min, after which high density and uniform nanotube networks are formed on top of the substrates. With the deposited semiconducting nanotube thin film acting as the conduction channel, the palladium source/drain extensions are patterned using e-beam writing to further shrink the device channel length down to 500 nm. As a final step, e-beam writing plus oxygen plasma is used to remove the unwanted nanotubes outside the device channel region in order to achieve accurate channel length and width and to remove the possible leakage in the devices.

Acknowledgment. We acknowledge financial support from Joint KACST/California Center of Excellence, and DARPA under Contract W31P4Q-10-C-0051 through the SBIR program. We thank Professor Mark Hersam of Northwestern University and Mr. Elliott Garlock and Dr. Nathan Yoder of Nanointegris for valuable discussions.

Supporting Information Available: Short-open-load-through (SOLT) de-embedding for the intrinsic RF performance (S1); DC and RF performance of the aligned nanotube RF transistors (S2); extrinsic and intrinsic h_{21} of the separated nanotube RF transistor under various gate biases (S3); hysteresis of the separated nanotube RF transistors (S4); near f_t two-tone intermodulation measurement (S5). This material is available free of charge *via* the Internet at http://pubs.acs.org.

REFERENCES AND NOTES

1. Durkop, T.; Getty, S. A.; Cobas, E.; Fuhrer, M. S. Extraordinary Mobility in Semiconducting Carbon Nanotubes. *Nano Lett.* **2004**, *4*, 35–39.
2. Zhou, X.; Park, J. Y.; Huang, S.; Liu, J.; McEuen, P. L. Band Structure, Phonon Scattering, and the Performance Limit of Single-Walled Carbon Nanotube Transistors. *Phys. Rev. Lett.* **2005**, *95*, 146805-1–146805-3.
3. Javey, A.; Guo, J.; Wang, Q.; Lundstrom, M.; Dai, H. Ballistic Carbon Nanotube Field-Effect Transistors. *Nature* **2003**, *424*, 654–657.
4. Javey, A.; Guo, J.; Farmer, D.; Wang, Q.; Yenilmez, E.; Gordon, R.; Lundstrom, M.; Dai, H. Self-Aligned Ballistic Molecular Transistors and Electrically Parallel Nanotube Arrays. *Nano Lett.* **2004**, *4*, 1319–1322.
5. Javey, A.; Guo, J.; Farmer, D.; Wang, Q.; Wang, D.; Gordon, R.; Lundstrom, M.; Dai, H. Carbon Nanotube Field-Effect Transistors with Integrated Ohmic Contacts and High-κ Gate Dielectrics. *Nano Lett.* **2004**, *4*, 447–450.
6. Bachtold, A.; Hadley, P.; Nakanishi, T.; Dekker, C. Logic Circuits with Carbon Nanotube Transistors. *Science* **2001**, *294*, 1317–1320.
7. Derycke, V.; Martel, R.; Appenzeller, J.; Avouris, P. Carbon Nanotube Inter- and Intramolecular Logic Gates. *Nano Lett.* **2001**, *1*, 453–456.
8. Liu, X.; Lee, C.; Han, J.; Zhou, C. Carbon Nanotube Field-Effect Inverters. *Appl. Phys. Lett.* **2001**, *79*, 3329–3331.
9. Javey, A.; Wang, Q.; Ural, A.; Li, Y.; Dai, H. Carbon Nanotube Transistor Arrays for Multistage Complementary Logic and Ring Oscillators. *Nano Lett.* **2002**, *2*, 929–932.
10. Chen, Z.; Appenzeller, J.; Lin, Y.; Oakley, J. S.; Rinzler, A. G.; Tang, J.; Wind, S. J.; Solomon, P. M.; Avouris, P. An Integrated Logic Circuit Assembled on a Single Carbon Nanotube. *Science* **2006**, *311*, 1735.
11. Cao, Q.; Kim, H. S.; Pimparkar, N.; Kulkarni, J. P.; Wang, C.; Shim, M.; Roy, K.; Alam, M. A.; Rogers, J. A. Medium-Scale Carbon Nanotube Thin-Film Integrated Circuits on Flexible Plastic Substrates. *Nature* **2008**, *454*, 495–500.
12. Wang, C.; Ryu, K.; Badmaev, A.; Patil, N.; Lin, A.; Mitra, S.; Wong, H.-S. P.; Zhou, C. Device Study, Chemical Doping and Logic Circuits Based on Transferred Aligned Single-Walled Carbon Nanotubes. *Appl. Phys. Lett.* **2008**, *93*, 033101-1–033101-3.
13. Ryu, K.; Badmaev, A.; Wang, C.; Lin, A.; Patil, N.; Gomez, L.; Kumar, A.; Mitra, S.; Wong, H.-S. P.; Zhou, C. CMOS: Analogous Wafer-Scale Nanotube-on-Insulator Approach for Submicrometer Devices and Integrated Circuits Using Aligned Nanotubes. *Nano Lett.* **2009**, *9*, 189–197.
14. Kang, S. J.; Kocabas, C.; Ozel, T.; Shim, M.; Pimparkar, N.; Alam, M. A.; Rotkin, S. V.; Rogers, J. A. High-Performance Electronics Using Dense, Perfectly Aligned Arrays of

Single-Walled Carbon Nanotubes. *Nat. Nanotechnol.* **2007**, *2*, 230–236.
15. Collins, P. G.; Arnold, M. S.; Avouris, P. Engineering Carbon Nanotubes and Nanotube Circuits Using Electrical Breakdown. *Science* **2001**, *292*, 706–709.
16. Engel, M.; Small, J. P.; Steiner, M.; Freitag, M.; Green, A. A.; Hersam, M. C.; Avouris, P. Thin Film Nanotube Transistors Based on Self-Assembled, Aligned, Semiconducting Carbon Nanotube Arrays. *ACS Nano* **2008**, *2*, 2445–2452.
17. Wang, C.; Zhang, J; Ryu, K.; Badmaev, A.; Gomez, L.; Zhou, C. Wafer-Scale Fabrication of Separated Carbon Nanotube Thin-Film Transistors for Display Applications. *Nano Lett.* **2009**, *9*, 4285–4291.
18. Wang, C.; Zhang, J.; Zhou, C. Macroelectronic Integrated Circuits Using High-Performance Separated Carbon Nanotube Thin-Film Transistors. *ACS Nano* **2010**, *4*, 7123–7132.
19. Li, S.; Yu, Z.; Yen, S.; Tang, W.; Burke, P. Carbon Nanotube Transistor Operation at 2.6 GHz. *Nano Lett.* **2004**, *4*, 753–756.
20. Louarn, A.; Kapche, F.; Bethoux, J.-M.; Happy, H.; Dambrine, G.; Derycke, V.; Chenevier, P.; Izard, N.; Goffman, M. F.; Bourgoin, J.-P. Intrinsic Current Gain Cutoff Frequency of 30 GHz with Carbon Nanotube Transistors. *Appl. Phys. Lett.* **2007**, *90*, 233108-1–233108-3.
21. Nougaret, L.; Happy, H.; Dambrine, G.; Derycke, V.; Bourgoin, J.-P.; Green, A. A.; Hersam, M. C. 80 GHz Field-Effect Transistors Produced Using High Purity Semiconducting Single-Walled Carbon Nanotubes. *Appl. Phys. Lett.* **2009**, *94*, 243505-1–243505-3.
22. Kocabas, C.; Kim, H.; Banks, T.; Rogers, J.; Pesetski, A.; Baumgardner, J.; Krishnaswamy, S.; Zhang, H. Radio Frequency Analog Electronics Based on Carbon Nanotube Transistors. *Proc. Natl. Acad. Sci. U.S.A.* **2008**, *105*, 1405–1409.
23. Kocabas, C.; Dunham, S.; Cao, Q.; Cimino, K.; Ho, X.; Kim, H.; Dawson, D.; Payne, J.; Stuenkel, M.; Zhang, H.; *et al.* High-Frequency Performance of Submicrometer Transistors That Use Aligned Arrays of Single-Walled Carbon Nanotubes. *Nano Lett.* **2009**, *9*, 1937–1943.
24. Arnold, M. S.; Green, A. A.; Hulvat, J. F.; Stupp, S. I.; Hersam, M. C. Sorting Carbon Nanotubes by Electronic Structure Using Density Differentiation. *Nat. Nanotechnol.* **2006**, *1*, 60–65.
25. Arnold, M. S.; Stupp, S. I.; Hersam, M. C. Enrichment of Single-Walled Carbon Nanotubes by Diameter in Density Gradients. *Nano Lett.* **2005**, *5*, 713–718.
26. Krupke, R.; Hennrich, F.; Löhneysen, H. V.; Kappes, M. M. Separation of Metallic from Semiconducting Single-Walled Carbon Nanotubes. *Science* **2003**, *301*, 344.
27. Wang, R.; Zhuge, J.; Huang, R.; Tian, Y.; Xiao, H.; Zhang, L.; Li, C.; Zhang, X.; Wang, Y. Analog/RF Performance of Si Nanowire MOSFETs and the Impact of Process Variation. *IEEE Trans. Electron Devices* **2007**, *54*, 1288–1294.
28. Pesetski, A. A.; Baumgardner, J. E.; Folk, E.; Przybysz, J. X.; Adam, J. D.; Zhang, H. Carbon Nanotube Field-Effect Transistor Operation at Microwave Frequencies. *Appl. Phys. Lett.* **2006**, *88*, 113103-1–113103-3.